SUPPLEMENTARY INFORMATION

Elucidating the Alkaline Oxygen Evolution Reaction Mechanism on Platinum

M. Favaro[1,2,3], C. Valero-Vidal[1,4], J. Eichhorn[3], F. M. Toma[3], P. N. Ross[5], J. Yano[2,6], Z. Liu[7,8] and E. J. Crumlin[1,4]*

[1] *Advanced Light Source, Lawrence Berkeley National Laboratory, One Cyclotron Rd., Berkeley, CA 94720, USA.*
[2] *Joint Center for Artificial Photosynthesis, Lawrence Berkeley National Laboratory, One Cyclotron Rd., Berkeley, CA 94720, USA.*
[3] *Chemical Sciences Division, Lawrence Berkeley National Laboratory, One Cyclotron Rd., Berkeley, CA 94720, USA.*
[4] *Joint Center for Energy Storage Research, Lawrence Berkeley National Laboratory, One Cyclotron Rd., Berkeley, CA 94720.*
[5] *Materials Sciences Division, Lawrence Berkeley National Laboratory, One Cyclotron Rd., Berkeley, CA 94720.*
[6] *Molecular Biophysics and Integrated Bioimaging Division, Lawrence Berkeley National Laboratory, One Cyclotron Rd., Berkeley, CA 94720.*
[7] *State key Laboratory of Functional Materials for Informatics, Shanghai Institute of Microsystem and Information Technology, Chinese Academy of Sciences, Shanghai 200050, People's Republic of China.*
[8] *School of Physical Science and Technology, ShanghaiTech University, Shanghai 200031, China.*

Supplementary Figure 1
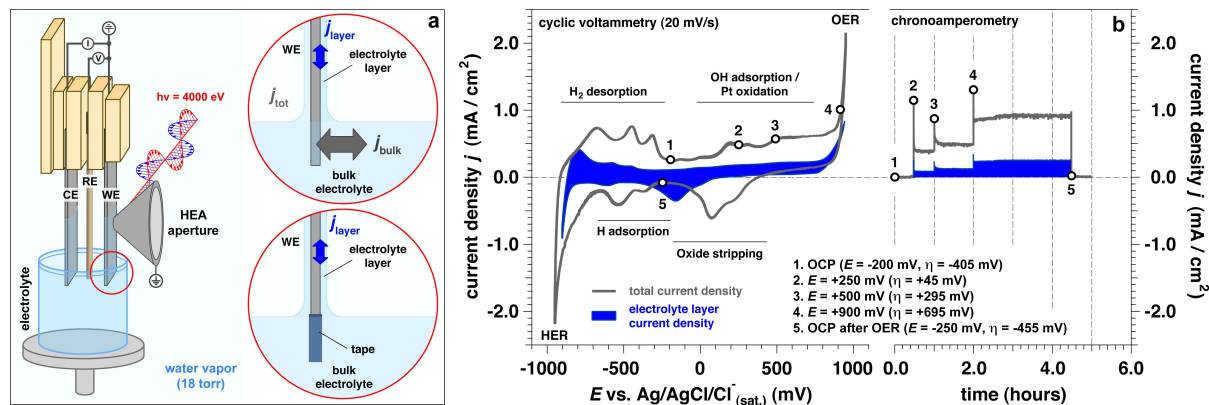
Experimental set-up and electrochemical characterization. **a**: three electrode electrochemical set up, showing the two different configurations (bare electrode and masked electrode) used in this work to unravel the electrochemical behavior of the nanometer-thick electrolyte layer (CE: counter electrode; RE: reference electrode; WE: working electrode, HEA: hemispherical electron analyzer); **b**: cyclic voltammetry (20 mV/s) and chronoamperometry for a polycrystalline Pt electrode in alkaline conditions (measured pH 13.9) at room temperature and for a water pressure in the chamber equal to 18 torr, acquired for the two configurations reported in Figure 1a (OCP: open circuit potential; HER: hydrogen evolution reaction; OER: oxygen evolution reaction).

Supplementary Figure 2
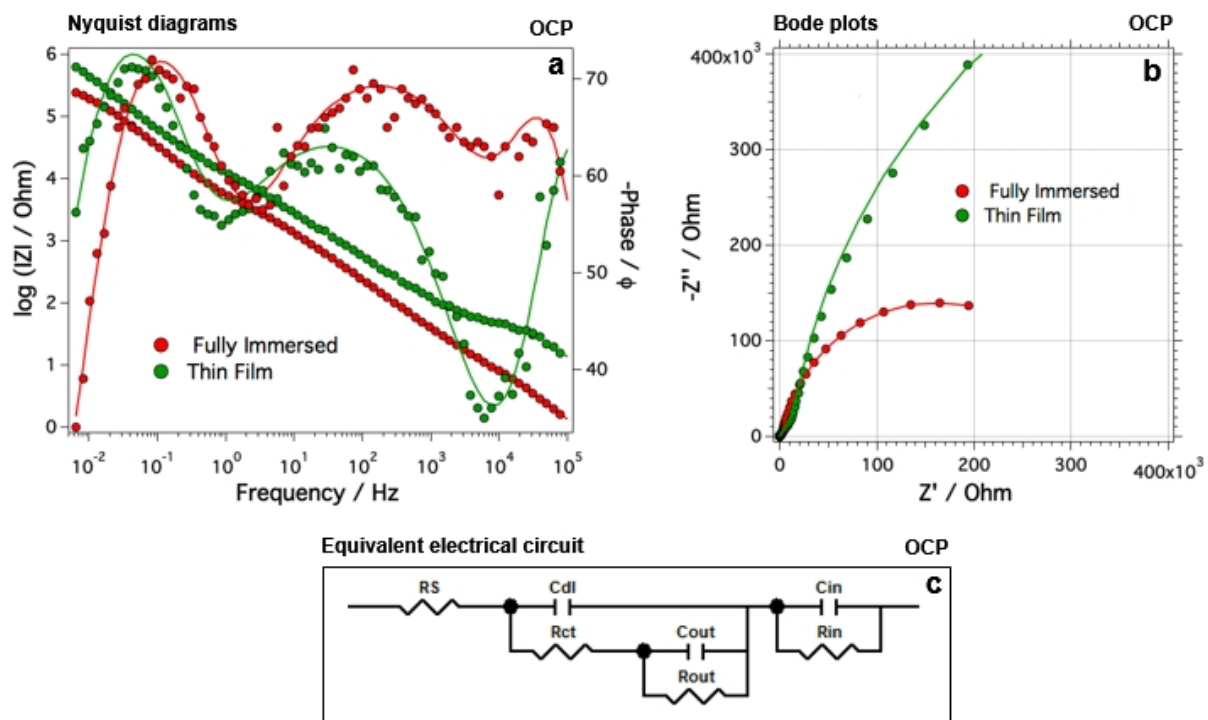
Nyquist diagrams (**a**) and Bode plots (**b**) (impedance modulus) of the Pt at OCP after dip and pull procedure with the WE fully immersed and isolating the thin electrolyte film; **c**: equivalent electrical circuit for the analysis of the impedance spectra.

Supplementary Figure 3
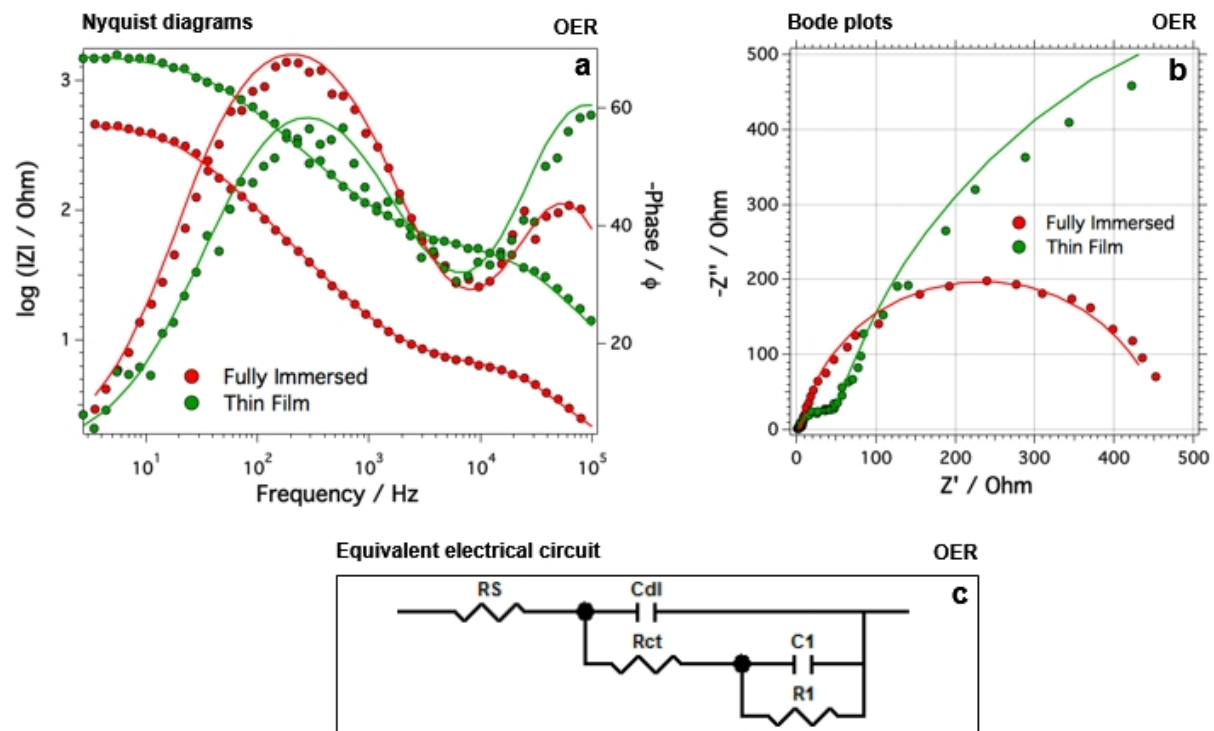
Nyquist diagrams (**a**) and Bode plots (**b**) of the Pt at +900 mV applied potential (OER conditions) after dip and pull procedure with the WE fully immersed and isolating the thin electrolyte film; **c**: equivalent electrical circuit for the analysis of the impedance spectra.

Supplementary Figure 4
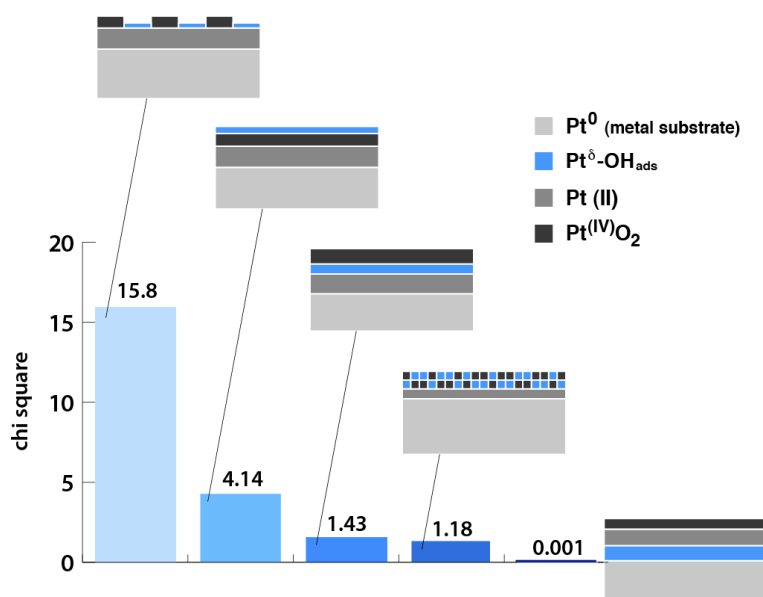
Significant models of platinum surface and corresponding chi-square values. Summary of the most significant models adopted in the numerical procedure used for the evaluation of platinum surface structure under the investigated experimental conditions. The simulation approach was performed using a variational principle, where the surface structure was obtained by the minimization of the chi-square between the experimental and simulated data.

Supplementary Figure 5
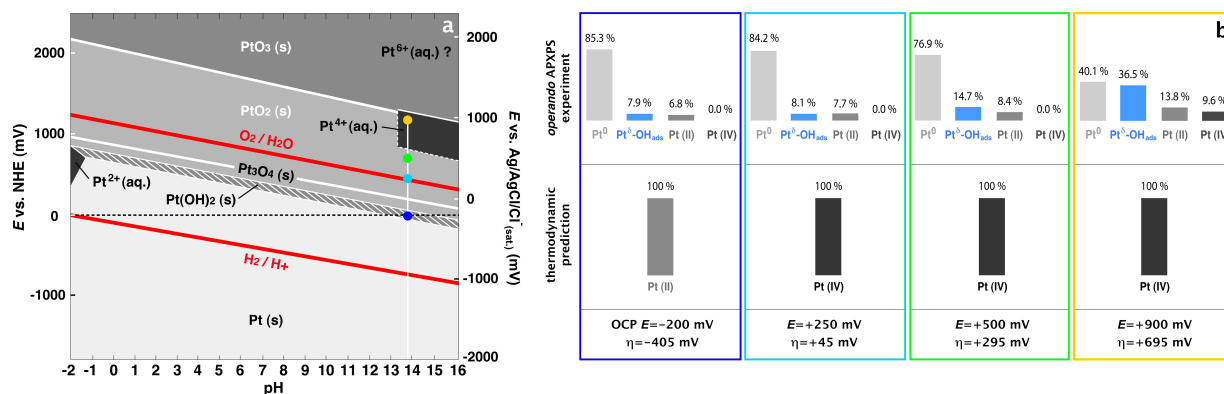
Comparison between thermodynamic predictions of platinum phase stability and surface chemistry studied with *operando* APXPS. **a**: Pourbaix diagram of the stability of platinum phases as a function of potential (E) and pH (the Pourbaix diagram was simulated by using the Materials Project facility). The red lines denote the thermodynamic range of stability of water. At high potential/pH the dissolution of Pt as Pt^{6+} cation is uncertained (1) (NHE: normal hydrogen electrode); **b**: comparison between thermodynamic predictions from Pourbaix diagram and Pt surface chemistry as a function of the applied potential experimentally accessed using *operando* APXPS (OCP: open circuit potential; OER: oxygen evolution reaction).

Supplementary Figure 6
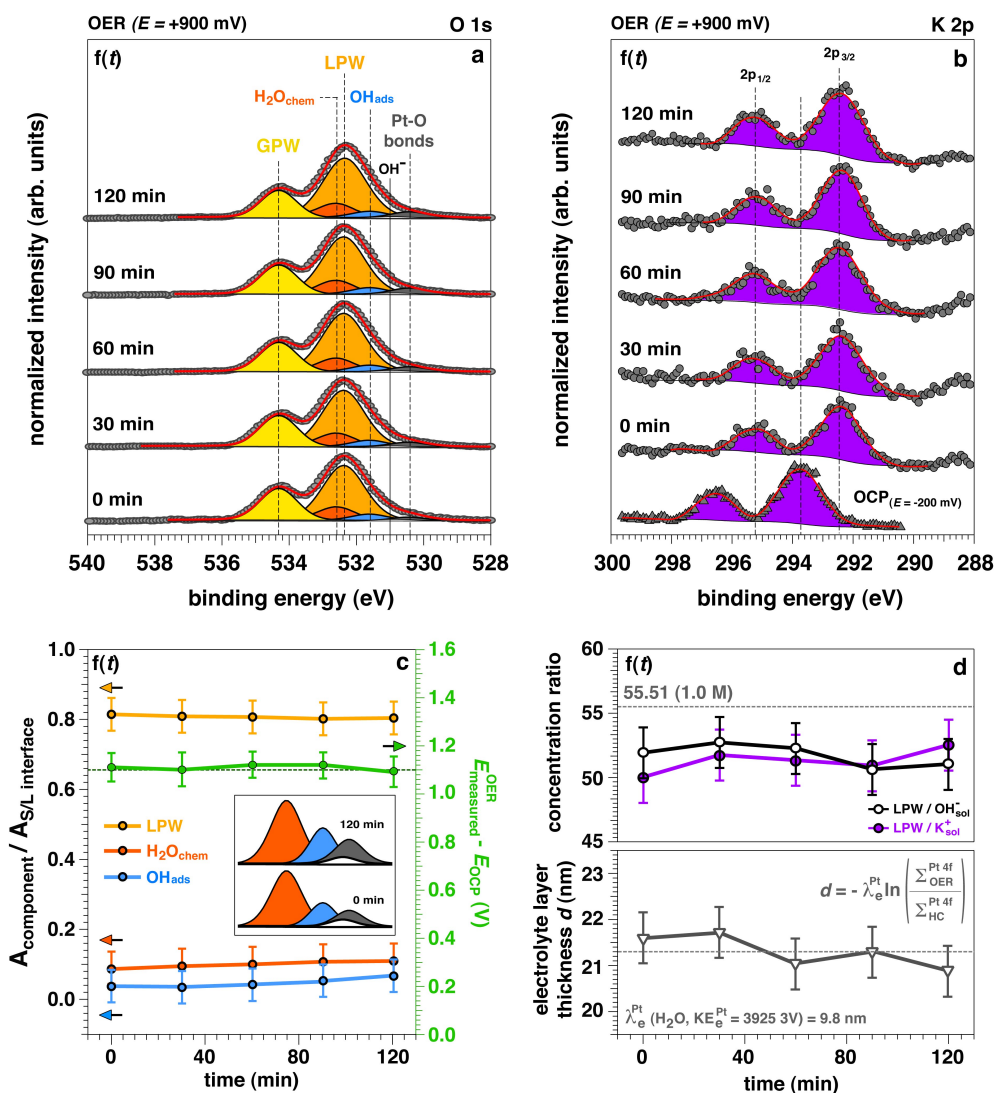
Time evolution investigation of the solid/liquid electrified interfaces under OER conditions; **a**, **b**: O 1s and K 2p core levels acquired as a function of the observation time (f(t)). **c**: reports the trend for liquid phase water (LPW), chemisorbed water (H_2O_{chem}) and adsorbed hydroxyls (OH_{ads}). The solid/liquid (S/L) interface components correspond to LPW, H_2O_{chem}, OH_{ads} and OH^- (hydroxyls in solution). The inset show a magnification of the low BE tail of the O 1s spectrum at t = 0 min and 120 min under OER conditions. It can be seen that the increase of the oxidation of the surface, together with the increase of the surface area as reported in the text, is accompanied by the corresponding slight increase of the chemisorbed water and hydroxyls. **d**: reports the trend of the ionic concentration as well as the thickness of the electrolyte layer on the Pt working electrode surface. Within the experimental uncertainty, these two quantities remain constant throughout the whole OER investigation as a function of the observation time (λ_e^{Pt}: inelastic mean free path for Pt 4f photoelectrons at a kinetic energy (KE) of 3925 eV; HC: hydrated conditions; Σ: integrated peak area).

Supplementary Table 1

Equivalent electrical circuit parameter of the Pt in 1.0 M KOH after dip and pull procedure at OCP in the different WE configurations.

Open Circuit Potential ($E = -200$ mV)		
Electrical Elements	Fully Immersed	Thin Film
R_s / Ω cm^2	1.5	6.25
R_{ct} / Ω cm^2	23.25	98.5
C_{dl} / $\mu\Omega^{-1}$ cm^{-2} s^n	0.61	0.05
R_{out} / kΩ cm^2	7.75	32.5
Q_{out}/ $\mu\Omega^{-1}$ cm^{-2} s^n	17	9.68
n_{out}	0.73	0.70
C_{out} / μF cm^{-2}	0.33	0.6
R_{in} / kΩ cm^2	800	3400
Q_{in}/ $\mu\Omega^{-1}$ cm^{-2}s^n	18.7	11.8
n_{in}	0.92	0.92
C_{in}/μF cm^{-2}	379.25	35.7
Rp / kΩ cm^2	808	3433
X^2	0.13	0.2

Supplementary Table 2

Equivalent electrical circuit parameter of the Pt in 1M KOH after dip and pull procedure at +900 mV applied potential (OER conditions) in the different WE configurations.

$E_{applied}$ = +900 mV (OER conditions)		
Electrical Elements	Fully Immersed	Thin Film
R_s / Ω cm^2	3.3	9.0
R_{ct} / Ω cm^2	15.3	125.8
Q_{dl} / $\mu\Omega^{-1}$ cm^{-2} s^n	0.50	0.06
n_{dl}	0.99	0.99
C_{dl} / μF cm^{-2}	0.50	0.06
R_1 / Ω cm^2	1135.0	3752.5
Q_1 / $\mu\Omega^{-1}$ cm^{-2} s^n	10.6	2.68
n_1	0.91	0.84
C_1 / μF cm^{-2}	12.8	5.5
Rp / Ω cm^2	1150.0	3878.8
X^2	0.11	0.58

Supplementary Discussion 1

EIS were measured in two different WE configurations: (*i*) after the dip and pull procedure forming a nanometric thick electrolyte layer on the WE surface and keeping immersed the bottom part of the electrode in the bulk electrolyte, and (*ii*) using a tape in the bottom part of the electrode isolating the formed thin electrolyte film from the bulk electrolyte still maintaining the electronic conductivity (meniscus). Configuration (*ii*) was designed in order to favor the acquisition of the current coming from the interface electrolyte/thin electrolyte film, and avoiding higher contribution from the electrode immersed in the bulk electrolyte.

- *Open Circuit Potential*

EIS spectra obtained at the OCP after the dip and pull procedure on the Pt with and without isolation of the nanometric thick electrolyte layer from the bulk electrolyte are shown in **Supplementary Figure 1**. Nyquist diagram **(a)** and Bode plots **(b)** are shown.

Three time constants can be predicted in those spectra, which can be modeled with three layers with different dielectric distribution and resistive properties. The electrical equivalent circuit (EEC) used to model the experimental data is represented in **Supplementary Figure 1c** and the theoretical simulated impedance parameters for both studied electrode configurations are reported in **Supplementary Table 1**. In this EEC, the first time constant is attributed to the double later (C_{dl})/interfacial charge transfer resistance (R_{ct}), combined *in parallel* with the porous outer oxide layer. The third time constant was assigned to the inner oxide film, which was added in series with the previous time constants. This model is coherent with the XPS core levels and with the numerical simulations obtained at OCP.

A constant phase angle element (CPE) was used to replace capacitor elements related to the oxide film in order to take into account the non-ideal behavior of those capacitive elements. This non-ideality can be due to different physical phenomena (surface heterogeneity such as surface roughness, impurities, dislocations or grain boundaries among others). These inhomogeneities are present on a microscopic level under the oxide phase. CPE is defined in impedance representation as:

$$1. \quad Z_{CPE} = [Q \cdot (i\omega)^n]^{-1}$$

where Q is the CPE element constant, ω is the angular frequency in (in rad s^{-1}), i^2=-1 is the imaginary number, and n in the CPE exponent.

Brug approach was used in order to transform the CPE element (ω^{-1} cm^{-2} s^n) into capacitive (F cm-^{2}) values:

$$2. \quad C_{eff} = \left[\frac{Q}{(R)^{(1-n)}}\right]^{1/n}$$

For anodic film growth, oxide layers with different dielectrical behavior can be approximated to a plate capacitor. Thus, the different capacitances can be related with the film thickness according to the expression:

$$3.\ C = \varepsilon \cdot \varepsilon_0 \cdot \frac{A}{d}$$

where ε is the relative dielectric constant of the layer, A is the active area, d is the film thickness and ε_0 is the permittivity of the vacuum (8.85×10^{-14} F cm^{-1}). Thickness approximation of outer and inner oxide film layers has been calculated using relation 3, and a dielectric constant for the platinum oxide of 6.5. Values reported for the oxides formed on the Pt using both configurations are: (*i*) d_{out}=1.7 nm and d_{in}= 9.5 nm (total thickness of the oxide film ~11.2nm), and for the configuration (*ii*) d_{out}=0.95 nm and d_{in}= 16 nm (total thickness ~17nm). Thus, it can be also confirmed that the thickness of the inner oxide film exceeds the outer one in a ratio of 5.6 and 16.8 for the electrode fully immersed and the electrode with the tape on the bottom part, respectively. It is also important to mention that characterization of a defective and non-uniform oxide film with a pure capacitor, as was carried out using with approach, can produce significant uncertainties. However, this method allows one to electrochemically characterize the presence of different oxide components formed on the metal surface with different dielectrical behavior/conductivity, and also to support the numerical simulations carried out by the XPS analysis.

Comparing the electrochemical parameters obtained for both configurations, a ratio of 3.37 in the polarization resistance between the thin film and the fully immersed electrode is obtained.

- *Oxygen Evolution Reaction*

In **Supplementary Figure 2a** and **b** EIS spectra obtained under OER conditions were depicted. In those, two capacitive loops displayed in the impedance diagram are clearly distinguished, which corresponds with two differentiate time constants at higher and lower frequency domain. The EEC used to model the experimental results was presented in **Supplementary Figure 2c**, providing the best fitting with the lowest X^2 value, and the most logical physical interpretation (accordingly to the individual electrical elements selected which represent the electrochemical processes of the system). The impedance of both time constant varied with the applied potential, thus indicating that both are related with the kinetics of the reaction. In addition, the proposed model is normally used for oxide anodes during oxygen evolution.

In the proposed EEC, one time constant is attributed to the charge transfer resistance (R_{ct}) /double layer capacitance (C_{dl}) in parallel combination with R_1/C_1 (equivalent resistance and capacitance associated with the adsorption of intermediates).

The theoretical simulated impedance parameters for the EIS obtained in Pt in presence of 1M KOH, after fitting the experimental data with the corresponding EEC, are summarized in **Supplementary Table 2**. In this case, also the capacitive elements were substitute by constant phase elements, and subsequently converted into capacitance using Brug's approach. In addition, due to the non-ideality of the capacitive element corresponding to the double layer, relation 4 was used to convert the constant phase element of the double layer to capacitive value:

$$4. \quad C_{dl} = \left[\frac{CPE_{dl}}{\left(R_S^{-1}+R_{ct}^{-1}\right)^{(1-n_{dl})}}\right]^{1/n_{dl}}$$

From the extracted parameters some observations can be drawn: (i) ratio of the polarization resistance (Rp=Rct+R1) of 3.4 was measured between the EIS obtained with the tape and the electrode full immersed, (ii) tape added on the bottom part reduce the capacitance elements one order of magnitude (increase of the theoretical thickness one order of magnitude), (iii) X^2 is relatively higher for a EIS fitting which is mainly due to the high scattering obtained in the spectra at lower frequencies for the experimental set-up.

References

1. Pourbaix, M. Atlas of electrochemical equilibria in Aqueous Solutions (National Association of Corrosion Engineers, 1974).